IUBMB *Life*, 63(5): 287–294, May 2011

Critical Review

Structural Heterogeneity and Ligand Gating in Ferric *Methanosarcina acetivorans* Protoglobin Mutants

Alessandra Pesce[1], Lesley Tilleman[2], Sylvia Dewilde[2], Paolo Ascenzi[3,4], Massimo Coletta[5,6], Chiara Ciaccio[5,6], Stefano Bruno[7], Luc Moens[2], Martino Bolognesi[8] and Marco Nardini[8]

[1]*Department of Physics, University of Genova, Genova, Italy*
[2]*Department of Biomedical Sciences, University of Antwerp, Antwerp, Belgium*
[3]*Department of Biology, University Roma Tre, Roma, Italy*
[4]*Interdepartmental Laboratory for Electron Microscopy, University Roma Tre, Roma, Italy*
[5]*Department of Experimental Medicine and Biochemical Sciences, University of Roma "Tor Vergata", Roma, Italy*
[6]*Interuniversity Consortium for the Research on Chemistry of Metals in Biological Systems, Bari, Italy*
[7]*Dipartimento di Biochimica e Biologia Molecolare, Università degli Studi di Parma, Parma, Italy*
[8]*Dipartimento di Scienze Biomolecolari e Biotecnologie and CIMAINA, Università degli Studi di Milano, Milano, Italy*

Summary

Protoglobin from *Methanosarcina acetivorans* C2A (*Ma*Pgb), a strictly anaerobic methanogenic Archaea, displays peculiar structural and functional properties within members of the hemoglobin superfamily. In fact, *Ma*Pgb-specific loops and a N-terminal extension (20 amino acid residues) completely bury the heme within the protein matrix. Therefore, the access of diatomic gaseous molecules to the heme is granted by two apolar tunnels reaching the heme distal site from locations at the B/G and B/E helix interfaces. The presence of two tunnels within the protein matrix could be partly responsible for the slightly biphasic ligand binding behavior. Unusually, *Ma*Pgb oxygenation is favored with respect to carbonylation. Here, the crucial role of Tyr(B10)61 and Ile(G11)149 residues, located in the heme distal site and lining the protein matrix tunnels 1 and 2, respectively, on ligand binding to the heme-Fe-atom and on distal site structural organization is reported. In particular, tunnel 1 accessibility is modulated by a complex reorganization of the Trp(B9)60 and Phe(E11)93 side-chains, triggered by mutations of the Tyr(B10)61 and Ile(G11)149 residues, and affected by the presence and type of the distal heme-bound ligand. © 2011 IUBMB

IUBMB *Life*, 63(5): 287–294, 2011

Additional Supporting Information may be found in the online version of this article.

Received 31 January 2011; accepted 9 March 2011

Address correspondence to: Prof. Marco Nardini, Dipartimento di Scienze Biomolecolari e Biotecnologie, Università degli Studi di Milano, Via Celoria 26, I-20131 Milano, Italy. Tel: ++39-02-5031-4898. Fax: ++39-02-5031-4895. E-mail: marco.nardini@unimi.it

ISSN 1521-6543 print/ISSN 1521-6551 online
DOI: 10.1002/iub.484

Keywords archaea heme-protein; *Methanosarcina acetivorans* protoglobin; crystal structure; heme reactivity; protein matrix tunnels.

Abbreviations GCS, globin coupled sensor; *Ma*Pgb, protoglobin from *Methanosarcina acetivorans* C2A; *Ma*PgbO_2, oxygenated ferrous *Ma*Pgb; Pgb, protoglobin; rms, root mean squared.

INTRODUCTION

Protoglobins (Pgbs) are single domain heme-proteins composed of ~195 amino acids, which are structurally related to hemoglobins and myoglobins as well as to the N-terminal domain of archaeal and bacterial globin coupled sensor (GCS) proteins. Pgbs could be either a putative GCS ancestor or, alternatively, a nonchimeric evolutionary branch of GCS (*1–5*). So far, two archaeal Pgbs have been characterized, namely, one from the obligate aerobic hyperthermophile *Aeropyrum pernix* (*2*) and one from the strictly anaerobic methanogen *Methanosarcina acetivorans* [protoglobin from *Methanosarcina acetivorans* C2A (*Ma*Pgb)] (*6*). Although functional issues are still unclear, these two archaeal Pgbs have been proposed to facilitate O_2 detoxification and/or to act as CO sensor/supplier in methanogenesis (*2, 6*).

*Ma*Pgb is folded into a 3-on-3 α-helical sandwich (*6*), closely resembling the globin domain of the heme-based O_2 sensor responsible for aerotaxis in aerobic *Bacillus subtilis* (*7*), and the GCS from the strictly anaerobic δ-Proteobacteria *Geobacter sulfurreducens* (*8*).

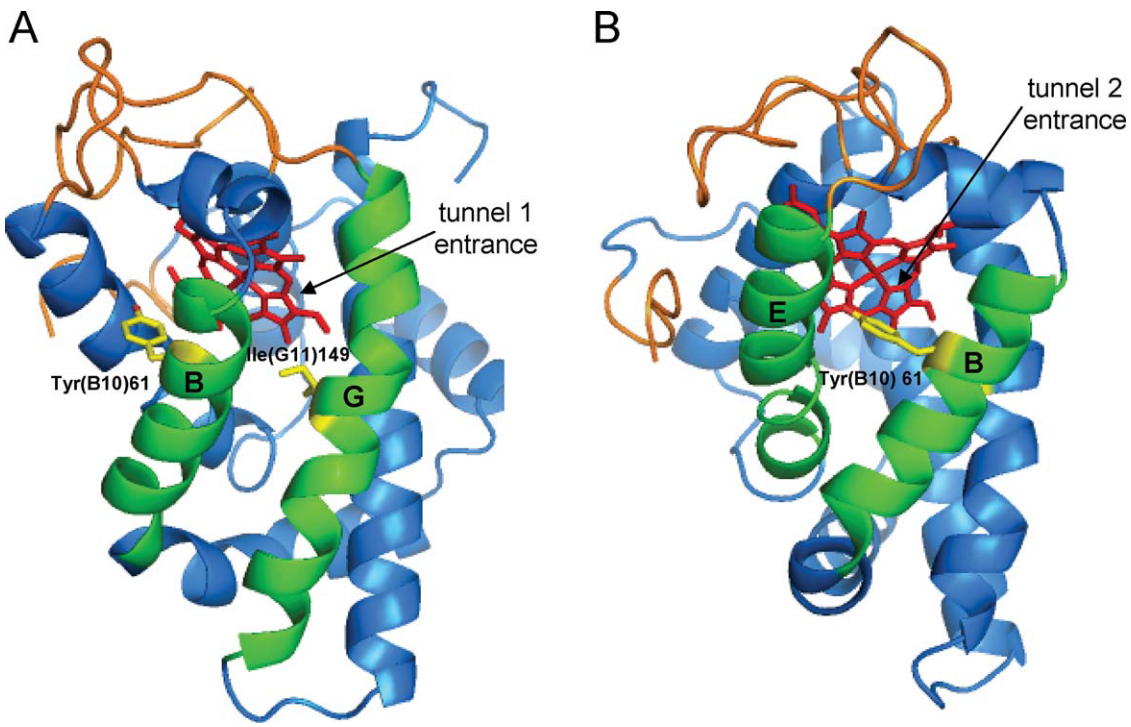

Figure 1. The *Ma*Pgb fold. Panels A and B highlight the helices flanking the entry of "tunnel 1" (B and G helices) and "tunnel 2" (B and E helices), respectively (in green), and the specific loops that bury the heme (in orange). The heme is shown in red. The protein is properly oriented in both panels, to bring each tunnel in the direction of sight; arrows indicate the location of the tunnel entry, for each panel. The mutated residues Tyr(B10)61 and Ile(G11)149 (the mutation sites) are shown, in ball and stick representation (in yellow). [Color figure can be viewed in the online issue, which is available at wileyonlinelibrary.com.]

Homodimeric *Ma*Pgb displays unusual functional and structural properties, as O_2 and CO binding are slightly anticooperative processes (*6*). Moreover, the heme is completely buried in the Pgb protein matrix and the diatomic ligand diffusion path to the heme pocket through the E7-gate is precluded. Therefore, the access of diatomic gaseous molecules, such as O_2, CO, and NO, to the heme cavity has been suggested to be granted by two orthogonal apolar tunnels reaching the heme distal site from locations at the B/G (tunnel 1; Fig. 1A) and B/E (tunnel 2; Fig. 1B) helix interfaces. Tunnel 1 (~7 Å in diameter, and ~16 Å in length) is lined by residues Ile(B5)56, Thr(B8)59, Trp(B9)60, Phe(B12)63, Phe(E11)93, Ile(E15)97, Phe(G7)145, Pro(G10)148, Ile(G11)149, Thr(G14)152, and Met(G15)153. Tunnel 2 (~5 Å in diameter, and ~10 Å in length) is a straight opening to the heme distal cavity nestled among residues Tyr(B10)61, Leu(B13)64, Gly(B14)65, Leu(C5)71, Phe(CD1)74, and Leu(E4)86. All residues lining the *Ma*Pgb tunnels are conserved in known Pgbs, suggesting functional implications for ligand diffusion to/from the heme cavity, for multiligand storage and/or for (pseudo-)enzymatic actions (*6*). The presence of two tunnels within the protein matrix could be partly responsible for the slightly biphasic behavior of CO binding of the *Ma*Pgb protein (k_{on1} = 5.0 × 10^6 M^{-1} sec^{-1} and k_{on2} = 2.4 × 10^6 M^{-1} sec^{-1}) (*6*).

Here, the role of the Tyr(B10)61 and Ile(G11)149 residues, located in the heme distal site and lining tunnels 1 and 2, respectively, is reported. The analysis of the three-dimensional structures of Tyr(B10)61 → Ala, Tyr(B10)61 → Trp, and Ile(G11)149 → Phe mutants highlights the role of the two tunnels within the protein matrix in channeling ligands to and from the heme-iron atom.

Tyr(B10)61: A GATE OF TUNNEL 2

Tyr(B10)61 is localized at the entrance of tunnel 2, a straight opening on the heme distal cavity nestled between the B- and the E-helices (Fig. 1B). Therefore, point mutations in this specific region have been designed to evaluate the structural impact on the heme distal site accessibility through tunnel 2 by increasing its aperture through the Tyr(B10)61 → Ala mutation, or by hindering its access through the Tyr(B10)61 → Trp substitution.

The tertiary structure of the Tyr(B10)61 → Ala and Tyr(B10)61 → Trp mutants are nearly identical in their backbone to those of the oxygenated ferrous *Ma*Pgb (*Ma*PgbO_2) and ligand-free ferric *Ma*Pgb (*6*), displaying root mean squared (rms) deviation values ≤0.43 Å, calculated for 190 C_α atom pairs (for ferric *Ma*Pgb the rms deviation has been averaged over the eight molecules present in the asymmetric unit). Simi-

Table 1
Data collection and refinement statistics for *Ma*Pgb mutants.

Data Collection	Tyr(61)B10 → Ala	Tyr(61)B10 → Trp	Ile(149)G11 → Phe
Space group	*C*2	*C*2	$P2_1$
Cell dimensions	a = 80.09 Å, b = 49.24 Å, c = 51.51 Å, β = 92.6°	a = 81.30 Å, b = 48.73 Å, c = 50.93 Å, β = 101.1°	a = 50.84 Å, b = 48.37 Å, c = 80.78 Å, β = 102.5°
Resolution (Å)	51.43–1.30 (1.37–1.30)[a]	50.00–2.40 (2.53–2.40)	78.81–2.20 (2.32–2.20)
Observations	144,189	18,515	70,356
Unique reflections	49,084	7,554	19,625
Completeness (%)	99.6 (99.8)	97.1 (98.3)	99.6 (99.9)
R_{merge}[b](%)	5.5 (25.5)	14.3 (31.6)	11.2 (28.3)
$I/\sigma(I)$	13.0 (3.6)	7.1 (2.8)	10.5 (5.9)
Multiplicity	2.9 (2.9)	2.5 (2.5)	3.6 (3.9)
Refinement			
R_{factor}/R_{free} (%)	13.2/16.4	23.8/30.6	23.9/31.6
Protein residues in the au	190	190	2 × 191
Heme groups	1	1	2
Water molecules	255	36	169
Phosphate ions	2	–	–
Glycerol	1	–	3
Isopropanol	–	–	1
Hepes	–	–	1
Model quality			
Overall *B*-factor (Å^2)	15.7	38.8	23.8
Rmsd from ideal values			
Bond lengths (Å)	0.012	0.007	0.009
Bond angles (°)	1.34	1.01	1.13
Ramachandran plot			
Most favored regions	93.5	85.1	91.5
Additional allowed regions	6.5	14.9	8.5

[b]Outer shell statistics are shown within parentheses.
[b]$R_{merge} = \Sigma_h\Sigma_i|I_{hi} - \langle I_h\rangle|/\Sigma_h\Sigma_i I_{hi}$.

larly, the quaternary assembly of the mutant proteins closely matches the dimeric assembly of *Ma*PgbO_2 and of ligand-free ferric *Ma*Pgb. The only significant structural differences of the protein backbone are localized in the 13–17 region, likely due to binding of a phosphate ion (from the crystallization solution) in *Ma*PgbO_2 (*6*) as well as in the ferric ligated *Ma*Pgb Tyr(B10)61 → Ala and Tyr(B10)61 → Trp mutants (present study), but not in the ferric unligated *Ma*Pgb (*6*). Moreover, the C_α backbone of the B helix (in the 55–62 region, around the mutation site) of the Tyr(B10)61 → Trp mutant is shifted away from the distal site cavity by about 0.98 Å relative to the same region of *Ma*PgbO_2 and of ferric ligand-free *Ma*Pgb. Data collection and crystallographic refinement statistics for *Ma*Pgb Tyr(B10)61 → Ala and Tyr(B10)61 → Trp mutants are reported in Table 1 (see also Experimental Procedures in Supporting Information).

THE UNEXPECTED LIGAND BINDING FEATURES OF THE Tyr(B10)61 → Ala MUTANT

The Tyr(B10)61 → Ala mutation has a dramatic impact on the accessibility of the heme distal site, by increasing the average tunnel diameter by more than 1.5 Å (with 6.4 Å the smallest distance between the Ala(B10)61 C_β atom and the surrounding residues). In the Tyr(B10)61 → Ala mutant structure, the tunnel 2 entrance hosts four bound water molecules, one of them matching the position of the Tyr(B10)61 OH-group in both *Ma*PgbO_2 and ligand-free ferric *Ma*Pgb (Fig. 2A). A wider tunnel entrance can allow the access of molecules bigger than diatomic ligands to the heme distal site. Indeed, in the Tyr(B10)61 → Ala mutant structure, an unexpected continuous electron density feature at the heme distal site was found, its size being significantly bigger than just a water molecule or a diatomic ligand (Fig. 3). At first inspection, the ring shape of such a feature (as displayed in the $2F_o - F_c$ electron

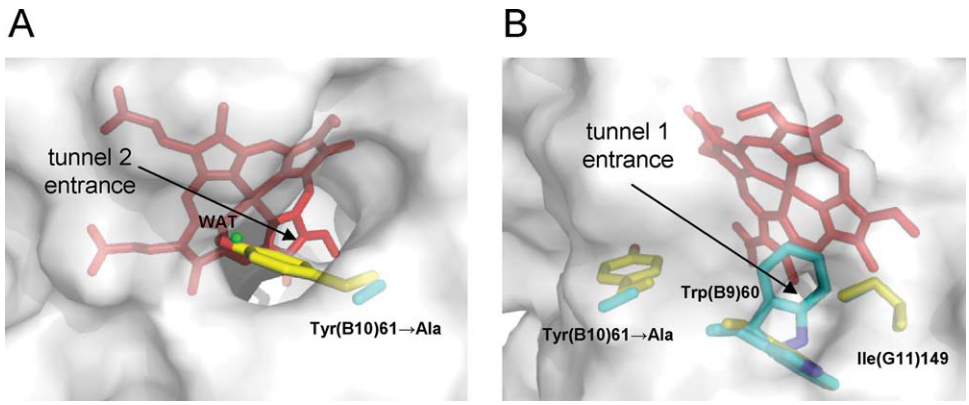

Figure 2. Tunnel entrances in *Ma*Pgb Tyr(B10)61 → Ala mutant. A: The widening of the tunnel 2 entrance is due to the Tyr(B10)61 → Ala mutation. B: The hindering of the tunnel 1 entrance is due to one conformer of the Trp(B9)60 side-chain. Residues from the *Ma*Pgb mutant and wild-type proteins are shown in cyan and yellow, respectively. The water molecule (WAT), that in the Tyr(B10)61 → Ala mutant overlaps the position of *Ma*Pgb Tyr(B10)61 OH-group, is shown as a green sphere. The protein molecular surface (as defined by a 1.4 Å radius probe) is displayed in semitransparent white color, allowing the view of underlying residues. For clarity, the protein tunnels are approximately oriented as in Fig. 1. [Color figure can be viewed in the online issue, which is available at wileyonlinelibrary.com.]

density map) suggested that the unassigned density might be compatible with an imidazole molecule of unknown origin, as the protein sample was not treated with imidazole during the purification/crystallization procedures. Furthermore, the electron density indicates that the molecule is coordinated to the ferric heme-Fe-atom, being relatively free of contacts from the rest of the protein (the closest protein atoms fall at 3.6 Å distance). When an imidazole molecule was modeled in the distal site, the R_{factor}/R_{free} values

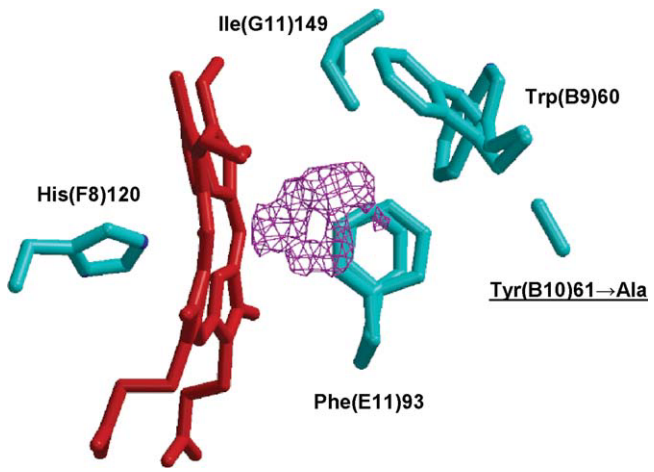

Figure 3. The unknown ligand bound to the *Ma*Pgb Tyr(B10)61 → Ala heme distal site. View of the Tyr(B10)61 → Ala mutant heme cavity including distal and proximal sites, and the $2F_o - F_c$ electron density (magenta mesh) calculated at the end of the refinement process (contoured at 1σ level). Residues lining the heme pocket are shown in cyan. The heme (in red) is seen edge on; the distal cavity is on the right of the heme. The mutant residue has been underlined. [Color figure can be viewed in the online issue, which is available at wileyonlinelibrary.com.]

improved slightly relative to the ligand-free refined structure (0.125/0.162 vs. 0.132/0.164), but the calculated electron density appeared still unsatisfactory, with difference Fourier map showing negative and positive density peaks located on the proposed ligand and toward the entrance of the distal site, respectively.

Based on the electron density shape, defined at 1.3 Å resolution (Fig. 3), and on the strong hydrophobicity of the *Ma*Pgb distal site cavity [lined by Phe(G7)145, Ile(G11)149, Phe(E11)93, Phe(CD1)74, Val(B13)64, Val(E7)89, Trp(B9)60, and Ala(B10)61], we propose that the unidentified heme-bound ligand is a small cyclic, possibly aromatic, compound. About the binding of uncommon heme ligands, it is worth noting that *Escherichia coli* flavohemoglobin and *Vitreoscilla* hemoglobin that host hydrophobic distal cavities [lined by Leu(E11), Phe(B9), and Tyr(B10)] have been reported to bind phospholipids and to interact efficiently with the phospholipid bilayer (*9, 10*). To provide first clues about the nature of the unknown ligand, we collected absorption spectra on the Tyr(B10)61 → Ala mutant crystals, which show a peak at 543 nm in both the ferric and ferrous form (Supporting Information Fig. 1SI). The peak shifts to 545 nm after treating the ferric form of the crystal with an excess of cyanide. Excluding the possibility of the endogenous hexacoordination of the heme-Fe-atom, the optical spectra indicate the presence of a distal ligand which absorbs at wavelengths typical of compounds coordinated to the heme-iron through a nitrogen atom, which can be displaced by cyanide, and which can bind similarly when the protein is in the ferric or ferrous forms. The analysis of the electron density shape (Fig. 3) and the optical spectra data (Supporting Information Fig. 1SI) suggest compounds such as nicotinic acid and analogues as the likely ligand found in the *Ma*Pgb Tyr(B10)61 → Ala mutant crystals, as reported for other globins (*11*).

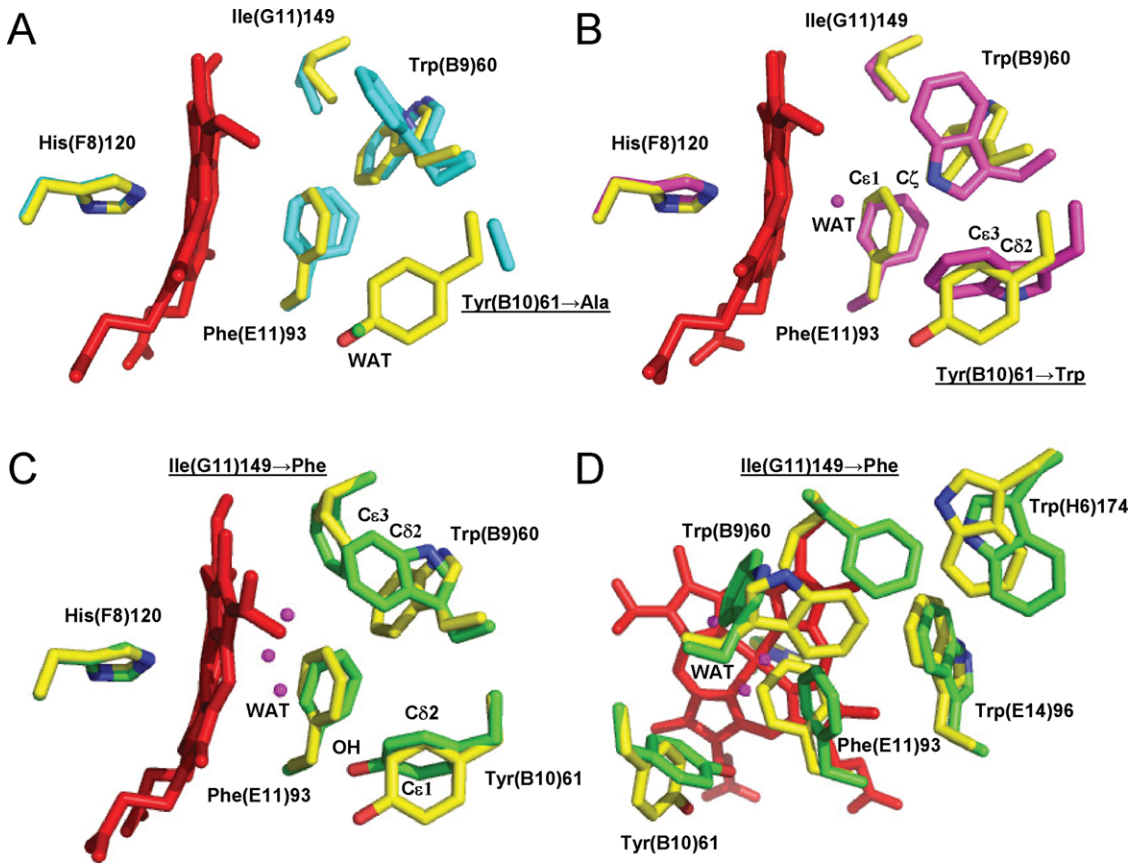

Figure 4. The heme distal site in *Ma*Pgb mutants. Residues lining the heme distal pocket are shown in yellow for the *Ma*PgbO$_2$ protein, in cyan for the Tyr(B10)61 → Ala mutant (A), in magenta for the Tyr(B10)61 → Trp mutant (B), and in green for the Ile(G11)149 → Phe mutant (C, D). The proximal His(F8)120 residue is also shown. A: The water molecule matching the position of the Tyr(B10)61 OH-group in *Ma*PgbO$_2$ is shown as a green sphere. B: The water molecule coordinated to the heme-iron is shown as a magenta sphere. C, D: The distal water molecules are shown as magenta spheres. The water molecule bound to the heme-Fe-atom in both (A) and (B) subunits of the Ile(G11)149 → Phe mutant is indicated as "WAT." D: The Ile(G11)149 → Phe distal site is shown from the tunnel 1 entrance to highlight the side-chain reorientation of neighboring residues due to the Ile(G11)149 → Phe mutation. Atoms with weak electron density are labeled (B, C). The mutated residues have been underlined. [Color figure can be viewed in the online issue, which is available at wileyonlinelibrary.com.]

The inspection of the heme distal cavity of the Tyr(B10)61 → Ala mutant provides also novel information relative to the dynamics of the aromatic residues there located. The absence of the Tyr(B10)61 side-chain has a profound impact in the relative orientation of the Phe(E11)93 and Trp(B9)60 side-chains, which both display double conformations that appear to be correlated to each other in order to avoid steric clashes between side-chains. Although the two coexisting conformation of Phe(E11)93 (occupancy of 0.5) differ only for a rotation of ~35° around the C_β—C_γ bond, one of the alternate conformations of the Trp(B9)60 side-chain (occupancy of 0.5) hinders tunnel 1 (Figs. 2B and 4A). It is worth noting that Phe(E11)93 mobility has been already observed in *Ma*PgbO$_2$, where the residue side-chain is affected by conformational disorder (*6*). On the contrary, Phe(E11)93 adopts a defined conformation in the ligand-free ferric *Ma*Pgb (*6*), where the fixed conformation of Phe(E11)93 triggers a rotation of about 45° of the Tyr(B10)61 side-chain relative to *Ma*PgbO$_2$, giving rise to a wider distal site cavity. Thus, the presence and the nature of the heme-bound ligand seem to have a deep impact on the architecture of the heme distal site and on its accessibility from the solvent phase, based on the relative orientation of the Trp(B9)60, Tyr(B10)61, and Phe(E11)93 side-chains.

As a whole, the Tyr(B10)61 → Ala mutation results in the expected widening of the tunnel 2 entrance, but strikingly it also promotes the reorganization of the Trp(B9)60 and Phe(E11)93 side-chains, resulting in partial hindering of tunnel 1.

HEME DISTAL SITE RESHAPING IN THE Tyr(B10)61 → Trp MUTANT

The heme-bound ligand in the Tyr(B10)61 → Trp mutant can be modeled as a water molecule whose coordination distance to the heme-Fe-atom is slightly higher than expected

(2.58 Å), and the ligand is not stabilized by any hydrogen bond involving distal site residues. Indeed, the only residue able to provide a polar interaction to the heme-bound water is Trp(B9)60, but even if its side-chain is pointing toward the distal site center (see below), the Nε1 atom is still too far from the ligand (3.85 Å) to stabilize it (Fig. 4B). The residue closest to the heme-bound water molecule is Phe(E11)93 (3.7 Å), which displays conformational disorder at the Cε1 and C_ζ atoms, likely to be ascribed to multiple side-chain rotamers around the C_α—C_β and C_β—C_γ bonds, as better observed in the 1.3 Å resolution structure of the Tyr(B10)61 → Ala mutant. It is worth noting that in *Ma*PgbO_2 the heme-bound O_2 molecule is also not stabilized by H-bonds to the protein, and Phe(E11)93 (at ~3 Å from the heme-bound O_2) is similarly affected by conformational disorder which, on the contrary, is not observed in the ferric ligand-free *Ma*Pgb (*6*).

The mutated Trp(B10)61 side-chain is partly disordered, with no density for the Cδ2 and Cε3 atoms (Fig. 4B). The modeled Trp side-chain matches the position occupied by Tyr(B10)61 in both *Ma*PgbO_2 and ligand-free ferric *Ma*Pgb (*6*), but with the side-chain rotated by 90° around the C_β—C_γ bond. Such Trp(B10)61 side-chain orientation would reduce by about 2 Å the diameter of the tunnel 2 entrance. However, considering the partial mobility of the Trp(B10)61 side-chain, as highlighted by its conformational disorder, it is likely that the Tyr(B10)61 → Trp mutation does not hinder significantly the ligand access to the heme distal site through tunnel 2. On the contrary, the mutation has a sizeable impact on the position of other distal site residues, as it induces a rotation of about 90° on both Phe(E11)93 and Trp(B9)60 side-chains, and a small reorientation (few degrees) of the Phe(B12)63 side-chain (Fig. 4B). As a consequence, Trp(B9)60 moves its side-chain toward the heme distal site center, thus hindering the ligand access through tunnel 1. This situation is reminiscent of that found in the heme distal site of the Tyr(B10)61 → Ala mutant (Fig. 2B). However, although the orientation of the Phe(E11)93 side-chain is superimposable in the two mutants, the orientation of the Trp(B9)60 side-chain in the Tyr(B10)61 → Trp mutant does not match the side-chain rotamer hindering tunnel 1 in the Tyr(B10)61 → Ala mutant (Fig. 4).

As a whole, the Tyr(B10)61 → Trp mutation while not restricting significantly the tunnel 2 entrance, on the contrary results in the unexpected hindering of tunnel 1, through a complex aromatic reorganization of side-chains involving Trp(B9)60 and Phe(E11)93 residues.

Ile(G11)149: A GATE OF TUNNEL 1

Ile(G11)149 is localized deeply inside tunnel 1, close to the heme pyrrole ring A (Figs. 1A and 2B). Therefore, the point mutation of this residue was designed to evaluate the structural impact on the heme distal site accessibility through tunnel 1 by hindering its access mutating Ile(G11)149 to Phe.

The Ile(G11)149 → Phe mutant crystallizes in the monoclinic space group $P2_1$, with two molecules in the asymmetric unit (molecules A and B) organized in a dimer whose quaternary assembly is identical to that found for *Ma*PgbO_2 and ferric ligand-free *Ma*Pgb (*6*). A superimposition of the C_α atoms (residues 5–195) of the A and B molecules reveals strong structural conservation within the dimer (rms difference 0.35 Å); therefore, all results discussed below apply to both subunits unless stated otherwise.

The structure of the Ile(G11)149 → Phe mutant is almost superimposable in its backbone to that of *Ma*PgbO_2 and of ligand-free ferric *Ma*Pgb (*6*) [rms deviation values being 0.35 Å and 0.51 Å, respectively, calculated for 189 C_α atom pairs (residues 6–195) and averaged over the two mutant subunits and over the eight subunits of the ligand-free ferric *Ma*Pgb]. Structural differences in the protein backbone are only localized at the 13–17 region, where in the Ile(G11)149 → Phe mutant no phosphate ion is bound, at the E-helix (residues 93–101), and at the GH hinge (residues 161–164). Data collection and crystallographic refinement statistics for the *Ma*Pgb Ile(G11)61 → Phe mutant are reported in Table 1 (see also Experimental Procedures in Supporting Information).

The heme distal site ligand in the Ile(G11)149 → Phe mutant has been modeled as a water molecule in both subunits, but with an elongated coordination bond to the ferric heme-Fe-atom. In subunit B, the water molecule is well defined by the electron density, at a distance of 2.9 Å from the heme-Fe-atom. In subunit A, the electron density of the ligand has an elongated shape, suggesting the presence of a water molecule in two alternate positions. The first position matches that of subunit B, at 2.9 Å from the heme-Fe-atom, whereas the second falls at a closer distance (2.6 Å) and is H-bonded (2.7 Å) to another distal site water molecule (not present in subunit B) (Fig. 4C). In both subunits, the heme distal site water molecules are not stabilized by any H-bonds to protein residues. Only van der Waals contacts are present, involving the Trp(B9)60 and Phe(E11)93 side-chains for the water molecule bound to the heme-Fe-atom, and Trp(B9)60 and Phe(G7)145 for the additional water molecule present only in subunit A (Fig. 4C).

The Ile(G11)149 → Phe mutation has a great impact on the side-chain orientation of aromatic residues lying at the heme distal site (Fig. 4D). Phe(G11)149 inserts its side-chain phenyl ring in a hydrophobic cavity lined by Trp(B9)60, Phe(E11)93, Trp(E14)96, Met(H5)173, Trp(H6)174, and Thr(H10)178. As a consequence, the four aromatic residues [Trp(B9)60, Phe(E11)93, Trp(E14)96, and Trp(H6)174] dramatically reorient their side-chains. Trp(E14)96 shifts aside by ~0.6 Å, together with the full E-helix, relative to *Ma*PgbO_2 (~0.3 Å relative to the ligand-free ferric *Ma*Pgb) (*6*). The Trp(H6)174 side-chain rotates ~30° around the C_α—C_β bond to avoid steric clashes to the Phe(G11)149 side-chain. Trp(B9)60 rotates its side-chain away of ~90°, occupying a site where in *Ma*PgbO_2 and in ligand-free ferric *Ma*Pgb a water molecule is located inside tunnel 1 (*6*). In such new orientation, the Trp(B9)60 side-chain shows poor density at the Cε2 and Cζ2 atoms. The Trp(B9)60 reorientation triggers a rotation of ~90° around the C_β-C_γ bond

of Phe(E11)93 (also affected by the shift of the E-helix), and a rotation toward the distal site of the Tyr(B10)61 side-chain. In this orientation, Tyr(B10)61 loses the hydrogen bonds between its OH-group and the Arg(E8)90 amide N and the Leu(E4)86 carbonyl O atoms, present in the ferrous and ferric *Ma*Pgb structures (*6*) (Fig. 4D). The absence of these interactions results in a partial disorder of the Tyr(B10)61 aromatic ring, with no electron density for the Cε1, Cδ2, and OH atoms in both subunits.

When compared with the structure of the Tyr(B10)61 → Ala and Tyr(B10)61 → Trp mutants, the side-chain positions of Trp(B9)60 and Phe(E11)93 in the Ile(G11)149 → Phe mutant are intermediate relative to the two alternate conformations found in the Tyr(B10)61 → Ala mutant for both residues (Fig. 4), whereas the Phe(E11)93 side-chain matches the position of that found in Tyr(B10)61 → Trp, with Trp(B9)60 having a different rotamer (Fig. 4C). Overall, the novel orientation of the Trp(B9)60 side-chain blocks the access to the distal site from tunnel 1, as found in the Tyr(B10)61 → Ala and Tyr(B10)61 → Trp mutants (Figs. 2B and 4D). Thus, the Ile(149)G11 → Phe mutation hinders tunnel 1 not directly, but through a remodeling of the distal site side-chain residues, especially Trp(B9)60. Additionally, the Ile(149)G11 → Phe mutation marginally alters tunnel 2, due to the rotation toward the distal site adopted by the Tyr(B10)61 side-chain which makes the solvent site access of tunnel 2 slightly more open (Fig. 4C).

CONCLUSIONS AND PERSPECTIVES

The structural analysis of the ferric forms of *Ma*Pgb mutants at residues Tyr(B10)61 and Ile(G11)149 sheds light on a number of structural details that may be important for the biological role of the protein. First, the strong hydrophobicity of the heme distal site seems to impair ligand stabilization by hydrogen bonding. Indeed, in the ferric Tyr(B10)61 → Trp and Ile(G11)149 → Phe mutants, a water ligand appears to be bound to the heme-iron, but with a coordination bond longer than expected without polar interaction(s) with heme distal site residues. Such absence of stabilizing interactions between the heme-bound ligand and distal residues strengthens the role assigned to the marked heme structural distortion on ligand affinity, as reported for O_2 binding to ferrous *Ma*Pgb (*6, 12*). Moreover, the shape and the size of the unknown ligand found in the Tyr(B10)61 → Ala distal site suggests that cyclic apolar (possibly aromatic) molecules other than "classical" diatomic ligands might be coordinated to the heme-iron in *Ma*Pgb. Indeed, recent data indicates that the *Ma*Pgb Tyr(B10)61 → Ala mutant can be co-crystallized with nicotinamide bound to the heme-Fe-atom at the distal site (our unpublished data). Whether this is also a property of wild type *Ma*Pgb and its functional implications will be the object of future investigations.

Second, the heme accessibility through the two tunnels that provide direct connections between the distal pocket and the solvent appear to be linked. In particular, mutations at Tyr(B10)61 (the entrance of tunnel 2) result in the unexpected hindering of tunnel 1, through a complex reorganization of side-chains involving Trp(B9)60 and Phe(E11)93.

Although in principle the existence of the two interconnected tunnels is suggestive of a possible dual path ligand exchange mechanism (typical of some enzymes) (*13*), the coupling of potential reactivity in the heme cavity with ligation is still to be explored. A detailed analysis of the dynamics and the nature of the structural crosstalk between the tunnels and of the possible role of the bound-ligand in modulating the accessibility to each tunnel will require further investigation. Present data identify three residues at key topological positions B9, B10, and E11 that appear to be involved in the dynamic regulation of ligand exchange between the solvent and the distal pocket. As a whole, the flexibility/adaptability of the heme distal site residues, whose aromatic side-chains are often found in multiple conformations, strongly suggests that additional residues may be involved in modulating ligand accessibility to the heme through both tunnels either directly or indirectly.

ACKNOWLEDGEMENTS

M.N. and M.B. are grateful to the University of Milano for supporting part of this investigation. This work was supported by grant from Fund for Scientific research (FWO, grant no. G.0247.09) to S.D. and L.M.

REFERENCES

1. Hou, S., Freitas, T. A. K., Larsen, R. W., Piatibratov, M., Sivozhelezov, V., Yamamoto, A., Meleshkevitch, E. A., Zimmer, M., Ordal, G. W., and Alam, M. (2001) Globin-coupled sensors: a class of heme-containing sensors in Archaea and Bacteria. *Proc. Natl. Acad. Sci. USA* **98**, 9353–9358.
2. Freitas, T. A. K., Hou, S., Dioum, E. M., Saito, J., Newhouse, J., Gonzalez, G., Gilles-Gonzalez, M.-A., and Alam, M. (2004) Ancestral hemoglobins in Archaea. *Proc. Natl. Acad. Sci. USA* **101**, 6675–6680.
3. Freitas,T. A. K., Saito, J., Hou, S., and Alam, M. (2005) Globin-coupled sensors, protoglobins, and the last universal common ancestor. *J. Inorg. Biochem.* **99**, 23–33.
4. Vinogradov, S. N., Hoogewijs, D., Bailly, X., Arredondo-Peter, R., Gough, J., Dewilde, S., Moens, L., and Vanfleteren, J. (2006) A phylogenomic profile of globins. *BMC Evol. Biol.* **6**, 31.
5. Vinogradov, S. N., Hoogewijs, D., Bailly, X., Mizuguchi, K., Dewilde, S., Moens, L., and Vanfleteren, J. (2007) A model of globin evolution. *Gene* **398**, 132–142.
6. Nardini, M., Pesce, A., Thijs, L., Saito, J. A., Dewilde, S., Alam, M., Ascenzi, P., Coletta, M., Ciaccio, C., Moens, L., and Bolognesi, M. (2008) Archaeal protoglobin structure indicates new ligand diffusion paths and modulation of haem-reactivity. *EMBO Rep.* **9**, 157–163.
7. Zhang, W. and Phillips, G. N. Jr. (2003) Structure of the oxygen sensor in *Bacillus subtilis*: signal transduction of chemotaxis by control of symmetry. *Structure* **11**, 1097–1110.
8. Pesce, A., Thijs, L., Nardini, M., Desmet, F., Sisinni, L., Gourlay, L., Bolli, A., Coletta, M., Van Doorslaer, S., Wan, X., Alam, M., Ascenzi, P., Moens, L., Bolognesi, M., and Dewilde, S. (2009) HisE11 and

HisF8 provide bis-histidyl heme hexa-coordination in the globin domain of *Geobacter sulfurreducens* globin-coupled sensor. *J. Mol. Biol.* **386**, 246–260.

9. Bonamore, A., Farina, A., Gattoni, M., Schinina, M., Bellelli, M. E., and Boffi, A. (2003) Interaction with membrane lipids and heme ligand binding properties of *Escherichia coli* flavohemoglobin. *Biochemistry* **42**, 5792–5801.
10. Rinaldi, A. C., Bonamore, A., Macone, A., Boffi, A., Bozzi, A., and Di Giulio, A. (2006) Interaction of *Vitreoscilla* hemoglobin with membrane lipids. *Biochemistry* **45**, 4069–4076.
11. Appleby, C. A., Wittenberg, B. A., and Wittenberg, J. B. (1973) Nicotinic acid as a ligand affecting leghemoglobin structure and oxygen reactivity. *Proc. Natl. Acad. Sci. USA* **70**, 564–568.
12. Bikiel, D. E., Forti, F., Boechi, L., Nardini, M., Luque, F. J., Martì, M. A., and Estrin, D. A. (2010) Role of heme distortion on oxygen affinity in heme proteins: the protoglobin case. *J. Phys. Chem. B* **114**, 8536–8543.
13. Milani, M., Pesce, A., Bolognesi, M., Bocedi, A., and Ascenzi, P. (2003) Substrate channeling: structural bases. *Biochem. Mol. Biol. Educ.* **31**, 228–233.